INTERNATIONAL JOURNAL FOR NUMERICAL METHODS IN FLUIDS
Int. J. Numer. Meth. Fluids 2007; **54**:1097–1117
Published online 16 January 2007 in Wiley InterScience (www.interscience.wiley.com). DOI: 10.1002/fld.1416

Stability of fluid–structure thermal simulations on moving grids

B. Roe[1], A. Haselbacher[2,*,†] and P. H. Geubelle[1]

[1]*University of Illinois at Urbana-Champaign, Urbana, IL 61801, U.S.A.*
[2]*Department of Mechanical and Aerospace Engineering, University of Florida, Gainesville, FL 32611, U.S.A.*

SUMMARY

This article analyses the stability of a thermally coupled fluid–structure interaction problem with a moving interface. Two types of fluid and structural discretizations are investigated: finite-difference/finite-difference as well as the more traditional finite-volume/finite-element (FV/FE) configuration. In either case, the material properties and grid spacing are treated as uniform within each domain. A theoretical stability analysis and corresponding numerical tests show that greater stability is associated with the algorithm in which the fluid domain is passed a Dirichlet condition and the solid domain a von Neumann condition and that the stability of the coupled scheme may be strongly affected by the interface velocity. Furthermore, it shows that the interface velocity has a larger destabilizing effect on the FV/FE discretization than on a finite-difference/finite-difference discretization. Copyright © 2007 John Wiley & Sons, Ltd.

Received 11 April 2006; Revised 9 November 2006; Accepted 10 November 2006

KEY WORDS: fluid–structure interaction; thermal coupling; numerical stability; boundary conditions

1. INTRODUCTION

The thermal interaction between fluid and solid domains is important in a wide range of multi-physics problems, such as heating of vehicles in hypersonic flow [1], heating and cooling of turbine blades in jet engines [2, 3], thermoelastic deformation of a structure due to aerodynamic heating [4], and the ignition of solid propellants in rockets [5, 6]. A key component of fluid–structure interaction (FSI) problems is the algorithm used for coupling the domains along the interface. Even among algorithms that produce accurate solutions, there may be significant differences in stability properties. Such differences are seen between loosely coupled and fully coupled schemes or between

*Correspondence to: A. Haselbacher, Department of Mechanical and Aerospace Engineering, University of Florida, 222 MAE-B, P.O. Box 116300, Gainesville, FL 32611-6300, U.S.A.
†E-mail: haselbac@ufl.edu

Contract/grant sponsor: Center for Simulation of Advanced Rockets at the University of Illinois at Urbana-Champaign/ Department of Energy through the University of California; contract/grant number: B523819

explicit and implicit schemes. Although the stability limits of algorithms in each sub-domain are well established, the stability restrictions imposed by the coupling algorithms themselves are often not well known. Furthermore, detailed knowledge of stability limitations imposed by the coupling algorithm is very important, because an instability might manifest itself only after a large amount of computational time, particularly in large simulations such as those presented in [6]. Despite the importance of establishing stability limits of thermal coupling algorithms, few authors have tackled this problem. The only substantial and general analysis appears to be that of [7]. The detailed characterization of the stability of thermal coupling algorithms used in FSI simulations is the focus of the present study, with particular emphasis on the effect of the interface motion.

In simulations that couple fluid and thermal solvers, a common practice is to pass one domain a temperature (Dirichlet) boundary condition and the other a heat flux (von Neumann) boundary condition. This problem was previously investigated by Giles [7] for the case of a fixed interface and using a one-dimensional (1-D) finite-difference (FD) formulation for each domain. However, the analysis presented in [7] is not able to capture the stability limit incurred by thermal coupling at a moving interface. Interface motion may arise if the solid deforms due to the loading by the fluid or if it regresses due to combustion, as in the case of solid propellants and other energetic materials [5, 6, 8]. Furthermore, typical solution methods for FSI computations are not based on FD, but rather on finite-volume/finite-element (FV/FE) methods for the fluid and structure, respectively. For these reasons, the work of Giles [7] is extended in two ways.

First, the effect of interface motion is included in the stability analysis. The partial differential equation corresponding to a 1-D conduction problem with a moving interface is

$$\rho C \frac{\partial T}{\partial t} + \rho C v_0 \frac{\partial T}{\partial x} = \kappa \frac{\partial^2 T}{\partial x^2} \tag{1}$$

where ρ is the density, C is the relevant specific heat, v_0 is the interface velocity, and κ is the thermal conductivity. Throughout this article, ρ, C, v_0, and κ are assumed to be constant. Equation (1) can be used to represent each domain, though the material parameters are not necessarily uniform across the interface. For the fluid domain, C is C_V, the specific heat at constant volume, and, for the solid domain, C is equal to the specific heat C_P. Following the convention adopted in [7], the domain which has passed the Dirichlet condition is represented by $+$ subscripts, while the domain which has passed the von Neumann condition is represented by $-$ subscripts.

The second extension of the work of Giles [7] is in the stability analysis of not only the FD case, but also of the more common FV/FE discretization. The remainder of this article is organized as follows. The analysis of the FD case is summarized in Section 2, which contains the derivation and numerical verification of a stability condition that incorporates non-zero interface velocity. This analysis is repeated in Section 3 for the FV/FE discretization for both moving and non-moving interfaces.

2. FINITE-DIFFERENCE DISCRETIZATION

Each domain in the system is discretized according to the FD formulation with grid spacings Δx_+ and Δx_-, see Figure 1. It is assumed that the mesh extends to infinity in both directions. As mentioned previously, the domains are discretized with a FD scheme: forward difference in time, a backward difference for the first spatial derivative, and a centred difference for the second spatial derivative.

DOI: 10.1002/fld

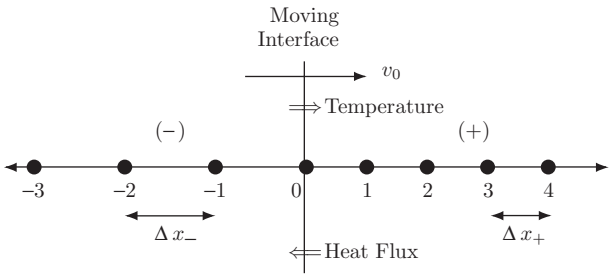

Figure 1. Schematic of discretized domain and node numbering. v_0 denotes the interface velocity.

2.1. Stability analysis

In the (−) domain ($x<v_0t$), the discretized version of (1) is

$$c_-\frac{T_j^{n+1}-T_j^n}{\Delta t}+c_-v_0\frac{T_j^n-T_{j-1}^n}{\Delta x_-}=\kappa_-\frac{T_{j+1}^n-2T_j^n+T_{j-1}^n}{\Delta x_-^2},\quad (j=0,-1,-2,-3,\ldots) \tag{2}$$

where

$$T_j^n=\begin{cases}T(j\Delta x_-,n\Delta t) & \text{if } j=0,-1,-2,\ldots\\ T(j\Delta x_+,n\Delta t) & \text{if } j=1,2,3,\ldots\end{cases} \tag{3}$$

Δt is the time step size and $c_\pm=\rho_\pm C_\pm$. In the (+) domain ($x>v_0t$), (1) takes the similar form:

$$c_+\frac{T_j^{n+1}-T_j^n}{\Delta t}+c_+v_0\frac{T_j^n-T_{j-1}^n}{\Delta x_+}=\kappa_+\frac{T_{j+1}^n-2T_j^n+T_{j-1}^n}{\Delta x_+^2},\quad (j=1,2,3,\ldots) \tag{4}$$

In order to pass thermal information from one domain to the other, the von Neumann condition is imposed on the left side (−) and the Dirichlet condition on the right side (+), referring to Figure 1. The flux q is computed at the left edge of the (+) domain to be passed to the (−) domain as a boundary condition. The discrete form of the heat-flux continuity condition at the interface ($x=v_0t$) is thus

$$c_-\frac{T_0^{n+1}-T_0^n}{\Delta t}+c_-v_0\frac{T_0^n-T_{-1}^n}{\Delta x_-}=\left(-q_+-\kappa_-\frac{T_0^n-T_{-1}^n}{\Delta x_-}\right)\frac{2}{\Delta x_-} \tag{5}$$

The flux is computed from (+) values in a first-order accurate manner as

$$q_+=-\kappa_+\left(\frac{T_1^n-T_0^n}{\Delta x_+}\right) \tag{6}$$

and is passed as the imposed interface heat flux to the (−) domain. Substituting (6) into (5) yields

$$c_-\frac{T_0^{n+1}-T_0^n}{\Delta t}+c_-v_0\frac{T_0^n-T_{-1}^n}{\Delta x_-}=\left[\kappa_+\left(\frac{T_1^n-T_0^n}{\Delta x_+}\right)-\kappa_-\left(\frac{T_0^n-T_{-1}^n}{\Delta x_-}\right)\right]\frac{2}{\Delta x_-} \tag{7}$$

DOI: 10.1002/fld

Because the problem considered here is not periodic, we cannot apply the usual von Neumann stability analysis. Instead, following Giles [7], the method of Godunov–Ryabenkii [9] is employed. In the Godunov–Ryabenkii method, the stability of (7) is analysed by the substitution

$$T_j^n = \begin{cases} z^n k_-^j & \text{if } j \leqslant 0 \\ z^n k_+^j & \text{if } j > 0 \end{cases} \tag{8}$$

Stability conditions can be established by requiring that $|k|<1$ and $|z|<1$. Further details can be found in [9, 10].

To facilitate the analysis, the following non-dimensional parameters are defined

$$r \equiv \frac{c_+ \Delta x_+}{c_- \Delta x_-} \tag{9}$$

$$d_\pm \equiv \frac{\kappa_\pm \Delta t}{c_\pm \Delta x_\pm^2} \tag{10}$$

and

$$\eta_\pm \equiv v_0 \frac{\Delta t}{\Delta x_\pm} \tag{11}$$

The parameters defined by (9) and (10) are identical to those used in [7], while the parameters defined by (11) correspond to the interface motion.

Focusing first on the (−) domain, (2) is solved for T_j^{n+1} and the dimensionless parameters d_- and η_- are substituted to give

$$T_j^{n+1} = T_j^n + d_-(T_{j+1}^n - 2T_j^n + T_{j-1}^n) - \eta_-(T_j^n - T_{j-1}^n) \tag{12}$$

Substituting (8) into (12) yields

$$z = 1 + d_-(k_- - 2 + k_-^{-1}) - \eta_-(1 - k_-^{-1}) \tag{13}$$

Applying the same steps to the (+) domain leads to

$$z = 1 + d_+(k_+ - 2 + k_+^{-1}) - \eta_+(1 - k_+^{-1}) \tag{14}$$

Shifting now to the discretized interface equation (7), which, when solved for T_0^{n+1} becomes

$$T_0^{n+1} = T_0^n + \frac{2\kappa_+ \Delta t}{c_- \Delta x_+ \Delta x_-}(T_1^n - T_0^n) - \frac{2\kappa_- \Delta t}{c_- \Delta x_-^2}(T_0^n - T_{-1}^n) - v_0 \frac{\Delta t}{\Delta x_-}(T_0^n - T_{-1}^n) \tag{15}$$

or, in terms of the non-dimensional parameters d, η, and r,

$$T_0^{n+1} = T_0^n + 2rd_+(T_1^n - T_0^n) - 2d_-(T_0^n - T_{-1}^n) - \eta_-(T_0^n - T_{-1}^n) \tag{16}$$

Substituting (8) into (16) gives

$$z = 1 + 2rd_+(k_+ - 1) - 2d_-(1 - k_-^{-1}) - \eta_-(1 - k_-^{-1}) \tag{17}$$

DOI: 10.1002/fld

Relations (13), (14), and (17) provide three equations for three unknowns: k_-, k_+, and z. To obtain an interface stability criterion, (13) and (14) are solved for k_- and k_+, respectively, and the resulting expressions substituted into (17). Solving (13) for k_- gives

$$k_-^{-1} = 1 - \frac{\eta_-}{d_- + \eta_-} - \frac{(1 - z - \eta_-)}{2(d_- + \eta_-)} \left[1 \mp \sqrt{1 - \frac{4d_-(1 - z)}{(1 - z - \eta_-)^2}} \right] \tag{18}$$

while (14) yields

$$k_+ = 1 - \frac{1 - z - \eta_+}{2d_+} \left[1 \mp \sqrt{1 - \frac{4d_+(1 - z)}{(1 - z - \eta_+)^2}} \right] \tag{19}$$

From (8), the conditions $|k_+|<1$ and $|k_-|>1$ ensure that the temperature remains finite for $j \to \pm\infty$. These requirements are fulfilled by taking the negative signs in (18) and (19). Inserting the corresponding expressions for k_+ and k_- into (17) gives

$$\begin{aligned} z = 1 + 2rd_+ & \left[1 - \frac{1 - z - \eta_+}{2d_+} \left(1 - \sqrt{1 - \frac{4d_+(1 - z)}{(1 - z - \eta_+)^2}} \right) - 1 \right] \\ & -(2d_- + \eta_-) \left\{ 1 - \left[1 - \frac{\eta_-}{d_- + \eta_-} - \frac{1 - z - \eta_-}{2(d_- + \eta_-)} \left(1 - \sqrt{1 - \frac{4d_-(1 - z)}{(1 - z - \eta_-)^2}} \right) \right] \right\} \end{aligned} \tag{20}$$

and, solving for r, this becomes

$$r = \frac{1 - z - \dfrac{2d_- + \eta_-}{2(d_- + \eta_-)} \left[2\eta_- + (1 - z - \eta_-) \left(1 - \sqrt{1 - \dfrac{4d_-(1 - z)}{(1 - z - \eta_-)^2}} \right) \right]}{(1 - z - \eta_+) \left[1 - \sqrt{1 - \dfrac{4d_+(1 - z)}{(1 - z - \eta_+)^2}} \right]} \tag{21}$$

For stability, it is required that $|z|<1$. Note that $z = 1$ produces the trivial solution, $r<\infty$. Therefore, the stability criterion is found by inserting $z = -1$ into (21), yielding the following inequality for stability of the coupled scheme:

$$r < \frac{2 - \dfrac{2d_- + \eta_-}{2(d_- + \eta_-)} \left[2\eta_- + (2 - \eta_-) \left(1 - \sqrt{1 - \dfrac{8d_-}{(2 - \eta_-)^2}} \right) \right]}{(2 - \eta_+) \left[1 - \sqrt{1 - \dfrac{8d_+}{(2 - \eta_+)^2}} \right]} \tag{22}$$

In the special case of a non-moving interface, (22) reduces to

$$r < \frac{\sqrt{1 - 2d_-}}{1 - \sqrt{1 - 2d_+}} \tag{23}$$

which is the original stability relation given in [7].

DOI: 10.1002/fld

Based on the analytical stability limit given by (22), it is possible to determine which of the common thermal data passing algorithms is more stable, i.e. which domain should be passed the temperature and which should be passed the heat flux. The most direct way to establish the stability is through the value of r. As r must be less than the right-hand side of the inequality to ensure stability, it is clear that decreasing the value of r has a positive effect on the stability of the simulation. Assuming similar grid spacings on either side of the interface, r is essentially the ratio of heat capacities. Also, since C_V for the fluid is generally of the same order as C_P for the solid, the magnitude of r essentially reduces to a ratio of densities. Because the density of a solid is typically much larger than that of a fluid, a small r is achieved by dividing the fluid density by the solid density. Referring to the schematic shown in Figure 1, this corresponds to the fluid domain being on the $(+)$ side and the solid domain on the $(-)$ side of the interface, i.e. a Dirichlet condition for the fluid and a von Neumann condition for the solid. The same conclusion was reached in [7] for the case of a non-moving interface.

2.2. *Numerical verification of stability analysis*

In order to verify the analytical results, a 1-D FD thermal solver was implemented based on (2), (4), and (7). Before attempting to confirm the generalized stability criterion given by (22) for moving interfaces, it is necessary to first ensure that the numerical results match the analytical stability limit for the non-moving interface. For the numerical test, the solid domain was given a uniform temperature of 1 K and the fluid domain was given a temperature of 2 K. At time $t=0$ the fluid domain is updated with T_0 given by the solid, returning q_+ as the boundary condition for the solid domain. Both domains are 1 m long with 100 nodes to ensure that end effects do not alter the behaviour of the interface. Adopting the values $d_\pm = \frac{3}{8}$, the stability criterion of (23) reduces to $r<1$. Figures 2(a) and (b) clearly show that the FD solver accurately follows the stability limit predicted by the analytical criterion (23).

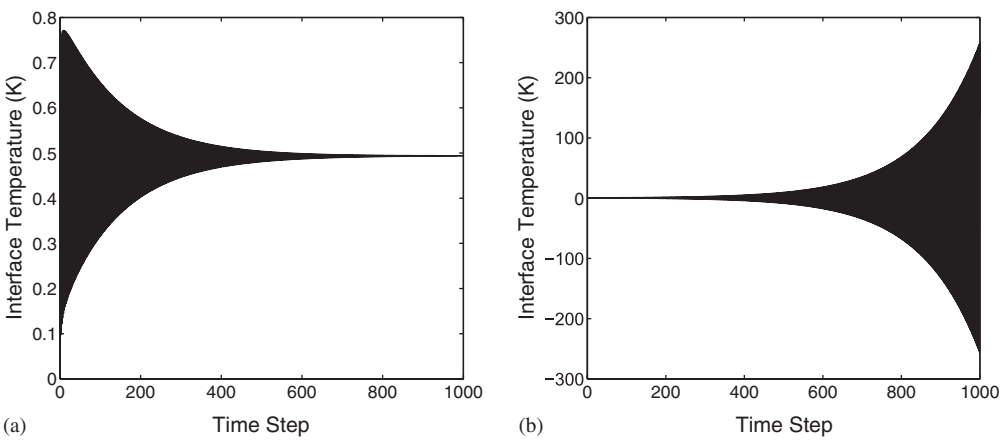

Figure 2. Evolution of the interface temperature for a stationary interface for the FD/FD discretization, and where $d_+ = d_- = \frac{3}{8}$: (a) $r = 0.99 < r_{\text{crit}} = 1$; and (b) $r = 1.01 > r_{\text{crit}} = 1$.

DOI: 10.1002/fld

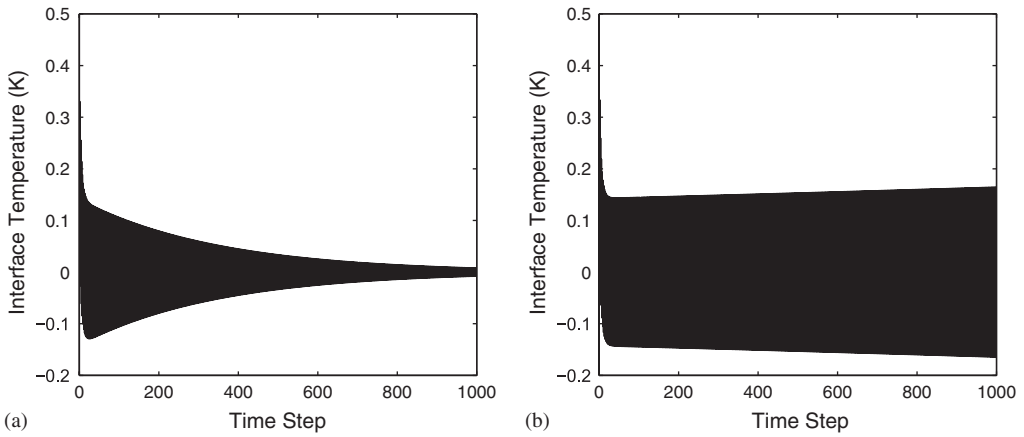

Figure 3. Evolution of the interface temperature for the case of a moving interface for the FD/FD discretization, with $d_+ = d_- = \frac{1}{4}$ and $\eta_+ = \eta_- = \frac{1}{2}$: (a) $r = 0.66 < r_{\text{crit}} = \frac{2}{3}$; and (b) $r = 0.667 > r_{\text{crit}} = \frac{2}{3}$.

Focusing now on the case of a moving interface, the stability criterion given by (22) shows that $r = \frac{2}{3}$ is the stability limit when $d_\pm = \frac{1}{4}$ and $\eta_\pm = \frac{1}{2}$. Figure 3(a) corresponds to a simulation using an r value of 0.66, which demonstrates stability as predicted. Similarly, in Figure 3(b), $r = 0.667$ and the interface temperature grows slowly, again as predicted. These two figures confirm the stability limit predicted by (22).

2.3. Discussion

Figure 4 presents the dependence of the critical time step value on the interface velocity, showing excellent agreement between analytical and numerical values. The detrimental effect of the interface motion on the stability of the numerical scheme is clearly demonstrated, as an increasing interface velocity requires a decrease in the time step to retain stability.

Through the stability criterion, the region of stability can be presented as a function of the dimensionless parameters that define the problem. Figures 5, 6(a), and 6(b) show the stability limits in the (d_+,d_-) plane for various values of r or $\eta_\pm$, where the stability region lies below each curve. The d_+ and d_- axes range from 0 to $\frac{1}{2}$ because the latter represents the stability limit for each sub-domain in the absence of coupling.

In Figure 5, the interface is stationary ($\eta_\pm = 0$) and each curve represents a different value of r. Clearly, r has a direct impact on the shape and size of the stability region. Taking $r = 1$ as the base value, Figure 5 shows that increasing r pulls the curve towards the d_- axis, while decreasing r pulls it towards the $d_- = \frac{1}{2}$ line. In the limiting case where $r = 0$, the stability region becomes the entire region $d_\pm \leqslant \frac{1}{2}$, which is the limit for each sub-domain in an uncoupled simulation. This result arises because, when r approaches zero, the product $c_-\Delta x_-$ approaches infinity, i.e. d_- tends to zero. The thermal solution in the $(-)$ domain then becomes stationary in time. Hence, the system is effectively decoupled and the stability limit of the $(+)$ domain becomes the only relevant criterion. For the opposite case, where r approaches infinity, the stability zone shrinks to zero; the simulation is unconditionally unstable. By the same reasoning, when r and, thus also, d_- approach infinity, the $(-)$ solution changes too rapidly for stability to be maintained.

DOI: 10.1002/fld

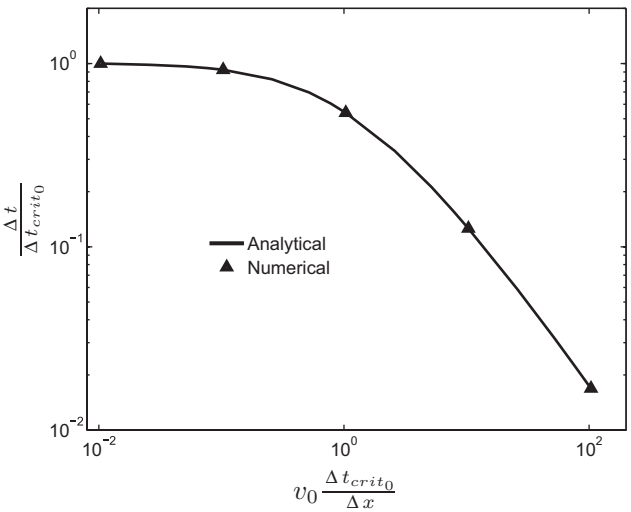

Figure 4. Effect of the interface velocity on the critical time step size for the FD/FD discretization. $\Delta x_+ = \Delta x_- = \Delta x$ and Δt_{crit_0} denote the critical value of the time step for a non-moving interface, as described by (23).

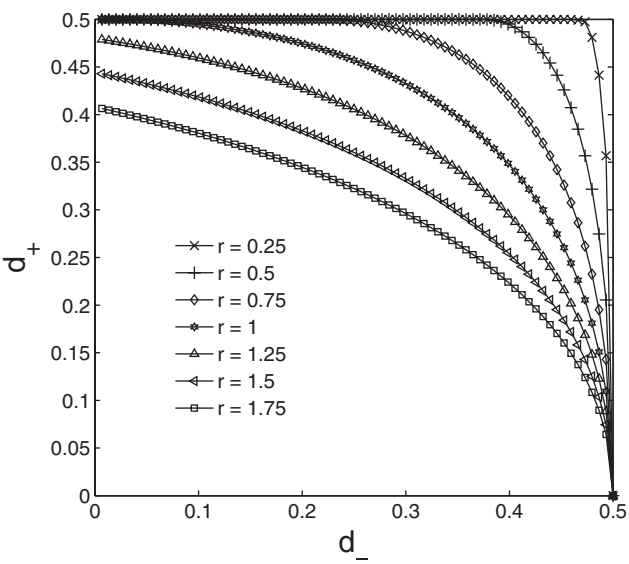

Figure 5. Effect of r on the predicted stability zones for the case of a stationary interface ($\eta_\pm = 0$) for the FD/FD discretization. The stability regions lie below the curves.

Figure 6(a) is similar to Figure 5, but the interface is not stationary ($\eta_\pm = \frac{1}{4}$). The overall shape of the curves is unchanged by the interface velocity even though they have been shifted down and to the left, effectively reducing the area of the stability region. The $\eta_\pm$ dependence of the limiting

DOI: 10.1002/fld

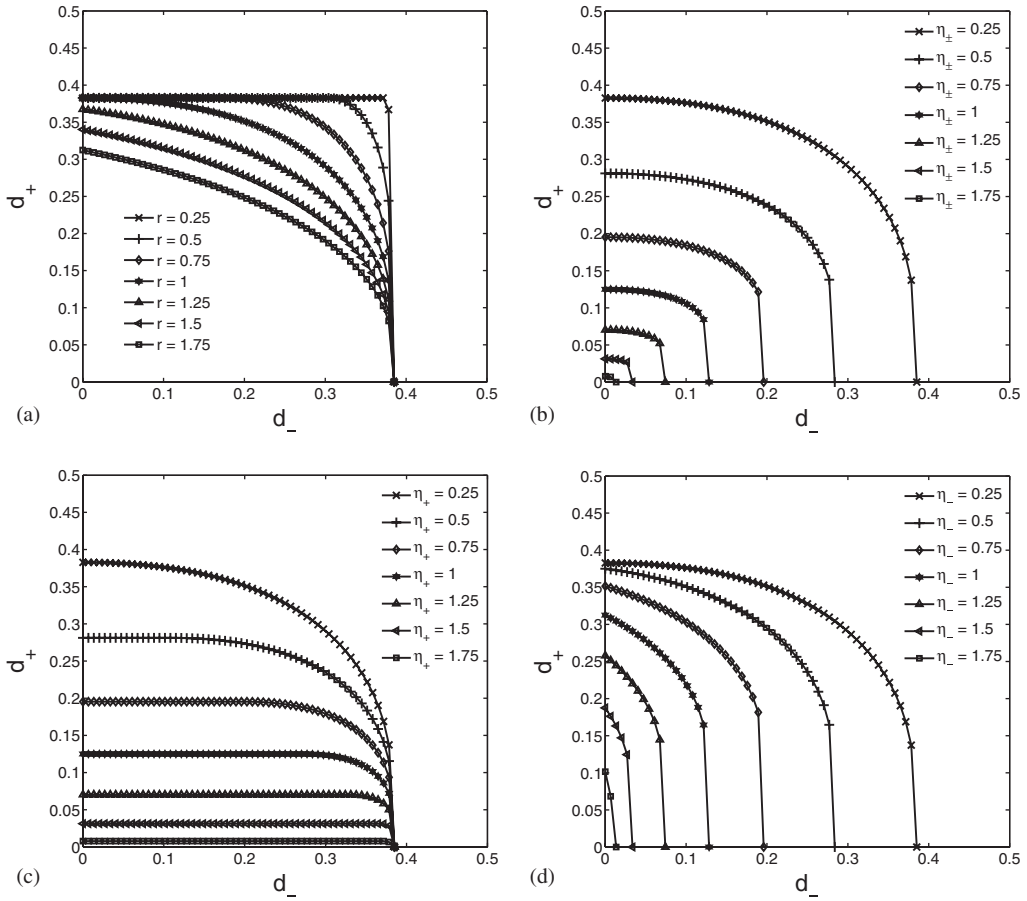

Figure 6. Predicted stability zones for the case of a moving interface for the FD/FD discretization: (a) $\eta_{\pm} = \frac{1}{4}$; (b) $r = 1$; (c) $r = 1$ and $\eta_{-} = \frac{1}{4}$; and (d) $r = 1$ and $\eta_{+} = \frac{1}{4}$.

value of $d_{\pm}$ arises from the terms

$$\sqrt{1 - \frac{8d_{\pm}}{(2 - \eta_{\pm})^2}} \tag{24}$$

appearing in (22). Therefore, the limiting cases are determined by

$$d_{\pm} = \frac{(2 - \eta_{\pm})^2}{8} \tag{25}$$

When $\eta_{\pm} = \frac{1}{4}$, $d_{\pm} = \frac{49}{128} \approx 0.383$, which matches the results shown in Figure 6(a). Physically, this new limit means that, for a specified system (fixed grids and material properties), increasing the interface velocity requires the time step to be reduced to maintain stability.

DOI: 10.1002/fld

Figure 6(b) shows the stability zones with $r = 1$ and as a function of $\eta_{\pm}$. Clearly, as $\eta_{\pm}$ increases, the stability region decreases as expected. For $\eta_{\pm} = 2$ the stability curve shrinks to a point at the origin, implying that no value of $d_{\pm}$ will give a stable result. The critical value arises because of the term $2 - \eta_{\pm}$ appearing in the denominator of (22). This indicates that the interface may move by, at most, two grid spacings per time step. This result is to be contrasted to the classical CFL (Courant–Friedrichs–Levy) condition for hyperbolic problems, which limits waves to travel only one cell per time step.

Figures 5 and 6(a) and (b), have reduced the stability problem from five parameters to four by assuming that $\eta_+ = \eta_-$. However, as the grid spacings in each domain are not required to be the same, the stability regions are now examined as η_+ and η_- vary independently. Figure 6(c) shows the stability regions with $r = 1$, $\eta_- = \frac{1}{4}$, and η_+ varying from 0.25 to 1.75. It was previously stated that the effect of increasing η_+ and η_- together is to shift the stability region down and to the left in the (d_+, d_-) plane. Figure 6(c) shows that varying only η_+ shifts the stability curve vertically. Similar results are demonstrated in Figure 6(d), in which η_- is varied, as changing η_- produces a horizontal shift in the stability zone. Although results have only been shown for the case where $\eta_{\pm} > 0$, similar conclusions will hold if $\eta_{\pm} < 0$.

3. FINITE-VOLUME/FINITE-ELEMENT DISCRETIZATION

Now a different discretization that is more conventional in FSI problems is considered: FE for the solid domain and FV for the fluid domain. Since the discretization of the fluid and solid domains is not the same for this system, the fluid domain is referred to as $+$ and the solid domain as $-$. This implicitly assumes that the fluid domain should be given the Dirichlet boundary condition and the solid domain given the von Neumann condition, as suggested previously by the study of the FD/FD discretization. The main difference, as shown in Figure 7, is in the discretization near the interface, where the centroid of the first fluid control volume is no longer located on the interface, but instead is offset by $\Delta x_+/2$. As will be shown below, this difference has important implications for the stability of the coupled scheme.

The semi-discrete FE formulation used to solve the 1-D heat equation in the solid domain is

$$[C]\{\dot{T}\} + [K]\{T\} = \{R\} \tag{26}$$

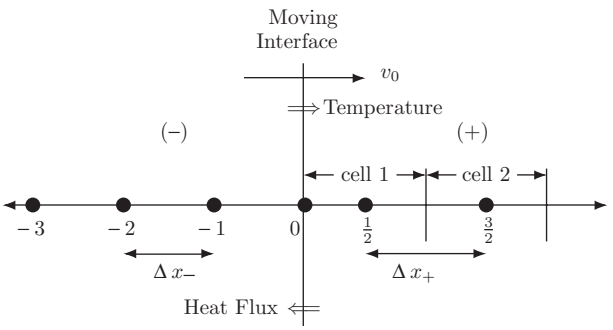

Figure 7. Schematic of discretized domain and node numbering for FV/FE discretization.

DOI: 10.1002/fld

where the vector $\{T\}$ contains the nodal temperature values

$$\{T\} = \langle T_0 \;\; T_{-1} \;\; T_{-2} \;\; \ldots \rangle^{\mathrm{T}} \tag{27}$$

$[C]$ is the lumped capacitance matrix, $[K]$ is the stiffness matrix, and $\{R\}$ is the load vector. For two-node 1-D thermal elements, these are

$$[C] = c_- \Delta x_- \begin{bmatrix} \frac{1}{2} & & & \\ & 1 & & \\ & & \ddots & \\ & & & \end{bmatrix} \tag{28}$$

$$[K] = \frac{\kappa_-}{\Delta x_-} \begin{bmatrix} 1 & -1 & & & \\ -1 & 2 & -1 & & \\ & -1 & 2 & -1 & \\ & & \ddots & \ddots & \ddots \\ & & & & \end{bmatrix} + \frac{c_- v_0}{2} \begin{bmatrix} -1 & 1 & & & \\ -1 & 0 & 1 & & \\ & -1 & 0 & 1 & \\ & & \ddots & \ddots & \ddots \\ & & & & \end{bmatrix} \tag{29}$$

and

$$\{R\} = \frac{\kappa_-}{\Delta x_-} \langle q_+ \;\; 0 \;\; \ldots \rangle^{\mathrm{T}} \tag{30}$$

All blank spaces in (28)–(30) represent zero entries. The discretization is completed by employing the forward Euler time integration scheme. For interior solid nodes, the fully discretized explicit thermal equation is thus

$$c_- \Delta x_- \frac{T_j^{n+1} - T_j^n}{\Delta t} + \frac{c_- v_0}{2}(T_{j+1}^n - T_{j-1}^n) - \frac{\kappa_-}{\Delta x_-}(T_{j+1}^n - 2T_j^n + T_{j-1}^n) = 0, \quad (j = -1, -2, \ldots) \tag{31}$$

Similarly, for the interface node, the discretized equation is

$$\frac{c_- \Delta x_-}{2} \frac{T_0^{n+1} - T_0^n}{\Delta t} + \frac{c_- v_0}{2}(T_0^n - T_{-1}^n) - \frac{\kappa_-}{\Delta x_-}(T_0^n - T_{-1}^n) = q_+ \tag{32}$$

where the interface flux passed by the fluid domain is

$$q_+ = \kappa_+ \left(\frac{T_{1/2}^n - T_0^n}{\frac{1}{2}\Delta x_+} \right) \tag{33}$$

DOI: 10.1002/fld

The FV formulation used to represent the fluid domain is obtained by integrating (1) with respect to x. For a single cell, the result is

$$c_+\Delta x_+ \left.\frac{\mathrm{d}T}{\mathrm{d}t}\right|_j^n + c_+ v_0 (T^n_{j+1/2} - T^n_{j-1/2}) = \kappa_+ \left(\left.\frac{\mathrm{d}T}{\mathrm{d}x}\right|_{j+1/2}^n - \left.\frac{\mathrm{d}T}{\mathrm{d}x}\right|_{j-1/2}^n \right), \quad \left(j = \frac{1}{2}, \frac{3}{2}, \ldots\right) \tag{34}$$

where j denotes the cell index. $T^n_{j\pm1/2}$ are computed by a simple average, while $\mathrm{d}T/\mathrm{d}x|^n_{j\pm1/2}$ are computed by a centred difference, with the exception of $j = \frac{1}{2}$, when T^n_0 is a boundary condition and $\mathrm{d}T/\mathrm{d}x|^n_0$ is given by a one-sided difference. Discretizing the time derivative with the forward Euler scheme gives

$$c_+ \frac{T^{n+1}_j - T^n_j}{\Delta t} = -\frac{1}{\Delta x_+} R^n_j \tag{35}$$

where the residual R^n_j is the net flux out of cell j at time step n.

Unlike the FD solution, the FV solution is not computed the same way in each cell. Because of the offset, the treatment of the first cell is

$$R^n_{1/2} = -\kappa_+ \frac{T^n_{3/2} - T^n_{1/2}}{\Delta x_+} + \kappa_+ \frac{T^n_{1/2} - T^n_0}{\Delta x_+/2} + c_+ v_0 \frac{T^n_{3/2} + T^n_{1/2}}{2} - c_+ v_0 T^n_0 \tag{36}$$

For all other cells, i.e. $j > \frac{1}{2}$, the residual is given by

$$\begin{aligned} R^n_j = &-\kappa_+ \frac{T^n_{j+1} - T^n_j}{\Delta x_+} + \kappa_+ \frac{T^n_j - T^n_{j-1}}{\Delta x_+} + c_+ v_0 \frac{T^n_{j+1} + T^n_j}{2} \\ &- c_+ v_0 \frac{T^n_j + T^n_{j-1}}{2}, \quad \left(j = \frac{3}{2}, \frac{5}{2}, \ldots\right) \end{aligned} \tag{37}$$

3.1. Non-moving interface

The stability criterion of the FV/FE discretization will first be derived for the simpler case of a stationary interface, for which the stability criterion for the FD scheme was given by (23).

3.1.1. Direct extension of [7] *to finite-volume/finite-element case.* To obtain the stability criterion for the case of the FV/FE discretization, the same method used in the FD/FD analysis is applied, i.e. determining k_- and k_+ assuming that they are uniform within their respective domains and substituting them into the interface relation. Beginning with the solid domain with $v_0 = 0$ in (31), the substitutions corresponding to (8) and the non-dimensional parameters given by (10) result in

$$z = 1 + d_-(k_- - 2 + k_-^{-1}) \tag{38}$$

or

$$k_-^{-1} = \frac{z - 1 + 2d_- \pm \sqrt{(1 - z - 2d_-)^2 - 4d_-^2}}{2d_-} \tag{39}$$

DOI: 10.1002/fld

To obtain k_+ only the solution for the first cell is needed. Therefore, substituting (36) into (35) with $v_0 = 0$ and solving for $T_{1/2}^{n+1}$ gives

$$T_{1/2}^{n+1} = T_{1/2}^n + d_+(T_{3/2}^n - 3T_{1/2}^n + 2T_0^n) \tag{40}$$

Together with (8), (40) leads to

$$z = 1 + d_+(k_+ - 3 + 2k_+^{-1/2}) \tag{41}$$

which can be expressed as a cubic equation for k_+. It can be shown that only one real solution for k_+ exists for (41) for all d_+.

The interface relation is obtained by substituting (33) into (32), setting $v_0 = 0$, and solving for T_0^{n+1}:

$$T_0^{n+1} = T_0^n + 4rd_+(T_{1/2}^n - T_0^n) - 2d_-(T_0^n - T_{-1}^n) \tag{42}$$

which, together with (8), leads to

$$z = 1 + 4rd_+(k_+^{1/2} - 1) - 2d_-(1 - k_-^{-1}) \tag{43}$$

Finally, solving for r and setting $z = -1$ leads to the stability criterion:

$$r < \frac{-2 + 2d_-(1 - k_-^{-1})}{4d_+(k_+^{1/2} - 1)} \tag{44}$$

Substituting (39) for k_- and (41) for k_+ into (44) with, as indicated before, $|k_+|<1$ and $|k_-|>1$ gives the analytical stability limits of the coupled FV/FE problem.

The accuracy of (44) can be established through direct comparison with a FE thermal solver using two-node elements coupled with a FV fluid solver. Figures 8(a) and (b) depict the variation of r_{crit} with d_- and d_+, respectively, where r_{crit} is given by (44). Figure 8(a) shows excellent agreement between numerical and analytical results for all values of d_-. However, Figure 8(b) shows that the numerically determined stability limit exhibits two distinct regimes. The first is an upward directed concave curve, where r_{crit} initially decreases with increasing d_+, reaches a minimum, and then increases. In the second regime, which exists when d_+ is greater than approximately 0.35 for the given case, the critical value of r decreases with increasing d_+.

The solid curve in Figure 8(b) represents the stability limit predicted by (44). This curve has the same U-shape as the first regime of the numerical data, and, for small values of d_+, the agreement with numerical results is very good. Figures 9(a) and (b) give insight into the level of agreement. With $d_+ = \frac{1}{10}$ and $d_- = \frac{1}{4}$, the predicted value of r_{crit} is 4.009. As expected, $r = 4$ gives a stable result while $r = 4.01$ is unstable. However, the analytical results fail to accurately follow the numerical data within the first regime for d_+ between roughly 0.25 and 0.35, and, after the transition to the second regime, fail to even capture the correct downward trend of the numerically determined r_{crit} values.

3.1.2. Spatially dependent k_+ and z. Figure 8(b) shows that the stability criterion, based on the assumption that k_+ is uniform in the fluid domain, produces inaccurate results with growing d_+ in the first regime and completely fails to capture the second regime. To improve the accuracy of the stability criterion, the assumption that k_+ be the same for each fluid cell is relaxed. In other words,

DOI: 10.1002/fld

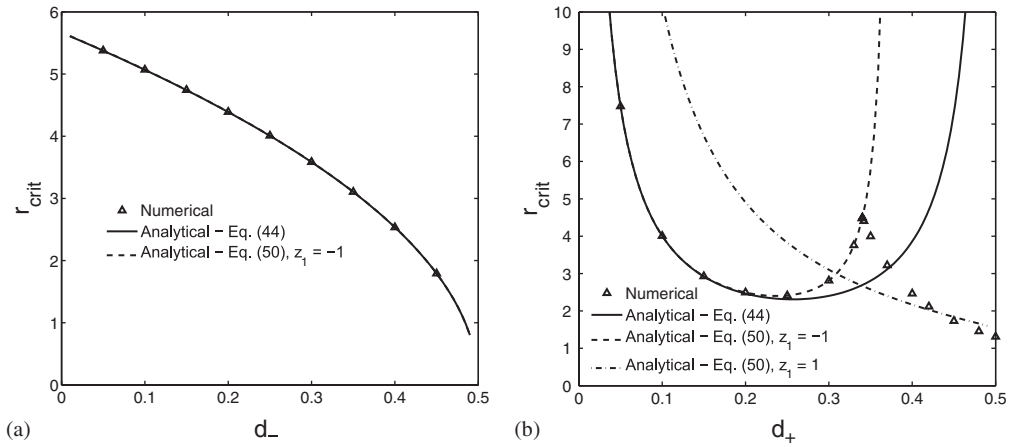

Figure 8. Numerical *versus* analytical stability limits for the FV/FE discretization with a non-moving interface with: (a) effect of d_- with $d_+ = \frac{1}{10}$; and (b) effect of d_+ with $d_- = \frac{1}{4}$.

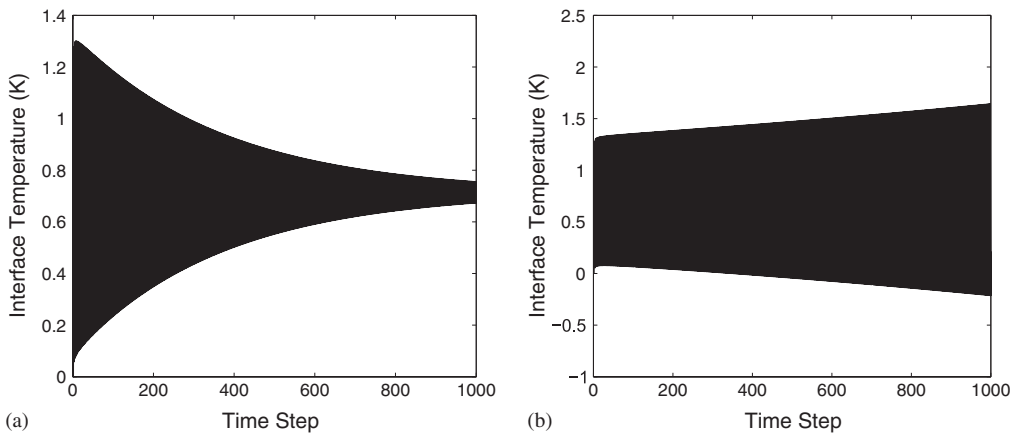

Figure 9. Evolution of the interface temperature for a stationary interface for the FV/FE discretization, and where $d_+ = \frac{1}{10}$ and $d_- = \frac{1}{4}$: (a) $r = 4 < r_{\text{crit}} = 4.009$; and (b) $r = 4.01 > r_{\text{crit}} = 4.009$.

it is no longer sufficient to use the solution for a single cell in determining k_+, as the value of k_+ at each location influences, and is influenced by, neighbouring cells. Therefore, the expression for k_+ at cell 1 must be derived by taking into account adjacent cells. The more the cells are included in the analysis, the more accurate the result is likely to be.

To determine an expression for k_+ in cell 1, including the influence of adjacent cells, k_+ is first determined for a cell sufficiently far from the interface. It is reasonable to assume that, for cells very far from the interface, the effect of the cell 1 discretization is very small. This means that k_+ reaches a constant value as $j \to \infty$. For an interior cell j, where j is sufficiently large, combining

DOI: 10.1002/fld

(35) and (37) with $v_0 = 0$, solving for T_j^{n+1}, and substituting the dimensionless parameters gives

$$T_j^{n+1} = T_j^n + d_+(T_{j+1}^n - 2T_j^n + T_{j-1}^n) \tag{45}$$

Using (8), this becomes

$$z_+ = 1 + d_+(k_+ - 2 + k_+^{-1}) \tag{46}$$

where z_+ represents the uniform value of z for fluid cells far from the interface. Equation (46) is exactly the same as the result of the FE implementation for the solid domain. This is a consequence of assuming a uniform grid and a centred approximation to the derivatives. Solving (46) for k_+ gives

$$k_+ = \frac{z_+ - 1 + 2d_+ \pm \sqrt{(1 - z_+ - 2d_+)^2 - 4d_+^2}}{2d_+} \tag{47}$$

Assuming that k and z are different for each cell, (40) can be rewritten as

$$z_1 = 1 + d_+\left[k_2^{3/2}k_1^{-1/2}\left(\frac{z_2}{z_1}\right)^n - 3 + 2k_1^{-1/2}\left(\frac{z_0}{z_1}\right)^n\right] \tag{48}$$

where k_1, k_2, z_1, z_2, and z_0, respectively, denote the values of k_+ and z in cells 1, 2, and at the interface, and n indicates the time level. Selecting $k_2 = k_+$ given by (47), the result, when inserted into (48) is

$$k_1 = \left\{\frac{z_1 - 1 + 3d_+}{d_+[(z_2/z_1)^n k_+^{3/2} + 2(z_0/z_1)^n]}\right\}^{-2} \tag{49}$$

which provides a new solution for cell 1 that can be substituted into the interface relation given below. This is the stability criterion attained by assuming that cell 1 is affected by adjacent fluid cells. The accuracy of the result depends on how many fluid cells are included in the analysis. For example, if only the first cell is considered, it is implicitly assumed that $k_2 = k_+$, which is the uniform value for the fluid. However, if the first two cells are taken into account, it is assumed that $k_3 = k_+$ which is used to solve for k_2, and finally, k_1. This process can be extended to any number of cells. Because k_+ for interior cells is negative for all values of d_+, k_1 must be a complex number. As an increasing number of cells are included in the analysis, the imaginary part of k_1 approaches zero and the stability criterion approaches a converged result.

Finally, the stability criterion for the case in which k and z are spatially dependent is

$$r < \frac{z_0 - 1 + 2d_-[1 - k_-^{-1}(z_-/z_0)^n]}{4d_+[k_1^{1/2}(z_1/z_0)^n - 1]} \tag{50}$$

Since $|z| < 1$ for stability, each z_j may be specified as 1 or -1. Setting $n = 1$ allows sign differences for various z to result in different solutions. Assuming that for each z in the expression for k_1 as well as z for the solid domain and z at the interface can be either 1 or -1, there are 64 resulting stability limits when three fluid cells are considered.

The dashed curve in Figure 8(b) represents the stability criterion based on (50) where k_1 is determined by taking the first three fluid cells into account and all $z_j = -1$. This curve is similar

DOI: 10.1002/fld

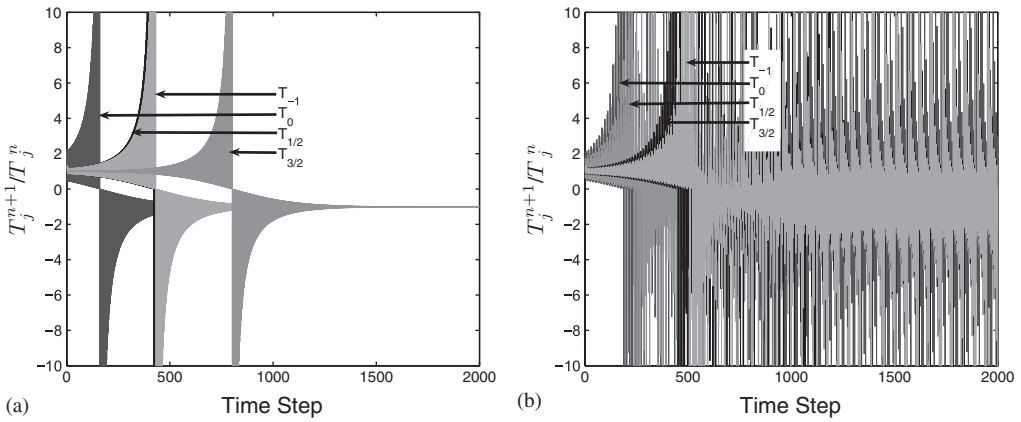

Figure 10. Evolution of T_j^{n+1}/T_j^n *versus* time for temperatures at and near the fluid–structure interface for a FV/FE simulation: (a) $d_+ = 0.146$ (first regime); and (b) $d_+ = 0.378$ (second regime).

in nature to the solid curve, however, it accurately follows the numerical results throughout the first regime. The dot-dashed curve in Figure 8(b) represents the stability limit based on k_+ again derived including three cells, where $n = 1$ and $z_- = -1$, $z_0 = -1$, $z_1 = 1$, $z_2 = -1$, $z_3 = -1$, and $z_4 = -1$, which is the closest fit for all possible combinations of z to the second d_+ regime. Unfortunately, for this region, the stability limit is only captured qualitatively, no matter how many fluid cells are included in the analysis.

The reasons for the discrepancy have so far eluded any investigation and might be associated with the difference in the numerical instability observed in the two regimes, as illustrated in Figures 10(a) and (b), which present the evolution of the ratio T_j^{n+1}/T_j^n at four positions in the vicinity of the interface ($j = -1, 0, \frac{1}{2}$, and $\frac{3}{2}$). Figure 10(a) shows the onset of instability in the first regime, for $d_+ = 0.146$ and r slightly greater than r_{crit}. Two observations can be made. First, the instability is truly driven by the interface, which first becomes unstable and is followed by the first fluid and solid nodes, as the instability propagates into each domain. Second, for all cases, the ratio T_j^{n+1}/T_j^n approaches -1 as $t \to \infty$. This justifies the assumption $z = -1$ that underlies the analysis that led to the analytical prediction described above.

Figure 10(b) corresponds to a simulation where $r > r_{\text{crit}}$ and $d_+ = 0.378$ is in the second regime. This figure is very similar to Figure 10(a), however, z does not approach a constant value as $t \to \infty$. It appears, based on the heavier shading in this region, that the average value of z in this case is still -1. However, the spurious oscillations suggest that perhaps $z = -1$ is not the only limit. Figures 11(a) and (b), which show the evolution of T_0^{n+1} *versus* T_0^n, give a better insight into the difference between the instability of the two regimes. In the first regime, represented by Figure 11(a), a linear relationship exists between T_0^{n+1} and T_0^n with time, where the slope is -1. In Figure 11(b) the evolution of T_0^{n+1} *versus* T_0^n for the second regime takes an elliptical form, where the major axis has a slope of -1. This reinforces the idea that the $z = -1$ limit, though present in the second regime, is not the only limit affecting the stability of the simulation. Furthermore, it might be an indication that the ansatz of the Godunov–Ryabenkii method (8) may no longer be valid for d_+ in the second regime.

DOI: 10.1002/fld

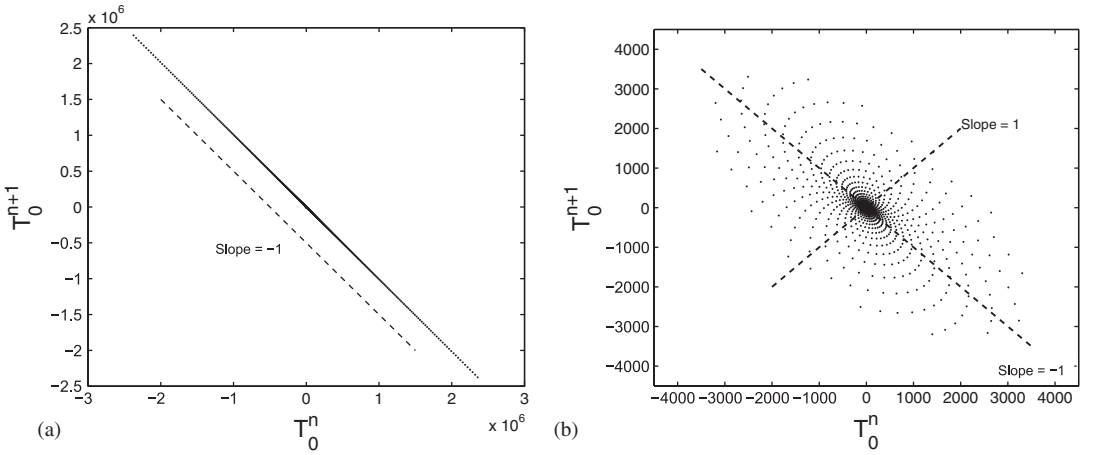

Figure 11. Evolution of T_0^{n+1} *versus* T_0^n for a FV/FE simulation: (a) $d_+ = 0.146$ (first regime); and (b) $d_+ = 0.378$ (second regime).

Though the form of the stability criterion for the FV/FE discretization is quite different from that of the FD/FD discretization, the conclusion regarding which data-passing algorithm is more stable remains the same. The coupling algorithm selection for the FD/FD discretization was based entirely on the fact that r must be less than some critical value. Because that fact is true for the FV/FE discretization as well, the conclusion remains valid. Therefore, as before, the fluid domain should be passed a Dirichlet boundary condition while the solid domain is passed a von Neumann condition.

3.2. Moving interface

A similar analysis can be performed for the moving interface case. Applying (8), (10), and (11) to (31), k_- becomes

$$k_-^{-1} = \frac{z_- - 1 + 2d_- \pm \sqrt{(1 - z_- - 2d_-)^2 - 4(d_-^2 - \eta_-^2/4)}}{2d_- + \eta_-} \tag{51}$$

For the fluid domain, combining (35) and (37) gives, with the aid of (8), (10), and (11),

$$k_+ = \frac{z_+ - 1 + 2d_+ \pm \sqrt{(1 - z_+ - 2d_+)^2 - 4(d_+^2 - \eta_+^2/4)}}{2d_+ - \eta_+} \tag{52}$$

To determine k_1 using three fluid cells, (35) and (37) are expressed for cells 2 and 3, as well as (35) and (36) for the first cell, assuming $k_4 = k_+$. Simultaneously solving these equations, the result for cell k_2 is

$$k_2 = \left(\frac{(z_2 - 1 + 2d_+)(z_3 - 1 + 2d_+) - (d_+^2 - \eta_+^2/4)}{(d_+^2 - \eta_+^2/4)(z_4/z_2)^n k_+^{7/2} + (d_+ + \eta_+/2)(z_1/z_2)^n (z_3 - 1 + 2d_+) k_1^{1/2}} \right)^{-2/3} \tag{53}$$

DOI: 10.1002/fld

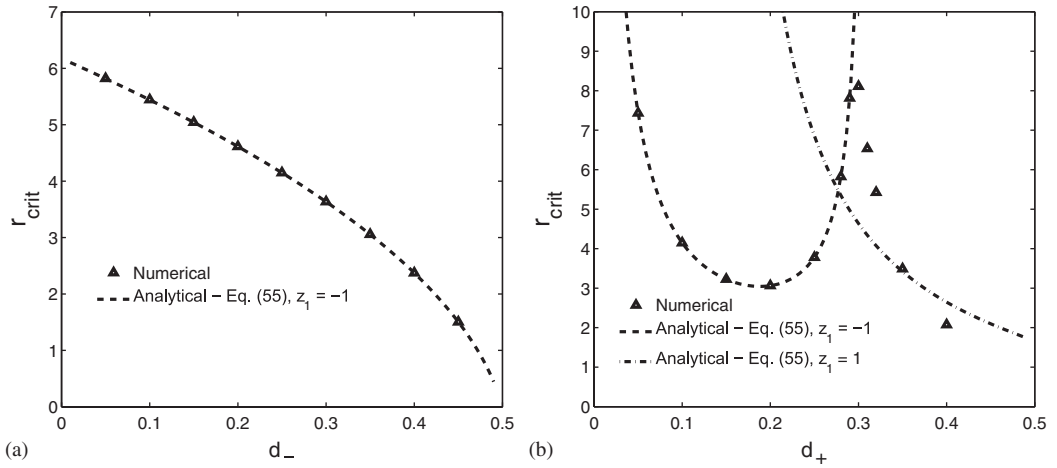

Figure 12. Numerical *versus* analytical stability limits for FV/FE discretization with a moving interface. $\eta_+ = \eta_- = \frac{1}{4}$ in both cases: (a) $d_+ = \frac{1}{10}$ while d_- varies; and (b) $d_- = \frac{1}{4}$ while d_+ varies.

while k_1 is given by

$$k_1 = \left(\frac{z_1 - 1 + 3d_+ + \eta_+/2}{(d_+ - \eta_+/2)k_2^{3/2}(z_2/z_1)^n + 2(d_+ + \eta_+/2)(z_0/z_1)^n} \right)^{-2} \tag{54}$$

This provides a stability criterion when inserted into the interface condition. The solution changes based on how many cells are used to compute k_2 and on the signs of the various z.

Combining (32) and (33), using the dimensionless parameters and (8), and solving for r gives

$$r < \frac{z_0 - 1 + (2d_- - \eta_-)[1 - k_-^{-1}(z_-/z_0)^n]}{4d_+[k_1^{1/2}(z_1/z_0)^n - 1]} \tag{55}$$

Substituting (54), based on (53) for k_1, gives multiple stability criteria, distinguished by varying the signs of z. Again, the positive roots in (51) and (52) must be chosen to ensure bounded temperature fields as $|x| \to \infty$.

In Figure 12 the variation of r_{crit} as a function of d_- and d_+ is shown, with $\eta_\pm$ held constant at $\frac{1}{4}$. Although the specific values of r are different here, when compared with Figure 8, the results are qualitatively the same. The r_{crit} *versus* d_+ curve again shows two distinct regimes, the first of which is captured well by the stability criterion using k_+ given by (54) with all $z = -1$, and the second, which is captured qualitatively but not matched quantitatively. As in the non-moving case, Figure 12(a) shows that d_- has no effect on the accuracy of the solution. Since the constant value of d_+ used lies within the first regime, agreement between the analytical and numerical stability limit is very good for all d_-.

Though Figure 12 shows good agreement between numerical and analytical results when d_+ is within the first regime, they represent only a single non-dimensional grid velocity. It is important to determine whether the value of $\eta_\pm$ affects the quality of the results. Figure 13 again shows r_{crit} *versus* d_+, however, multiple curves are shown, each representing a different value of $\eta_\pm$. As $\eta_\pm$ increases, the r_{crit} curve shifts upward and the width of the first regime decreases, i.e. the transition

DOI: 10.1002/fld

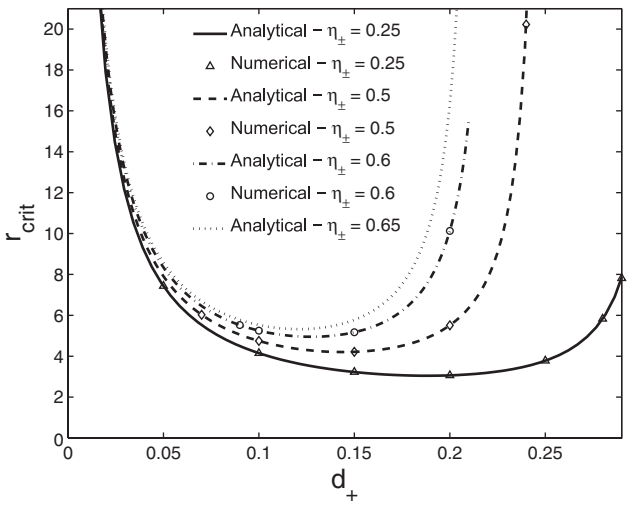

Figure 13. Effect of $\eta_\pm$ on the stability of the FV/FE discretization with $d_- = \frac{1}{4}$.

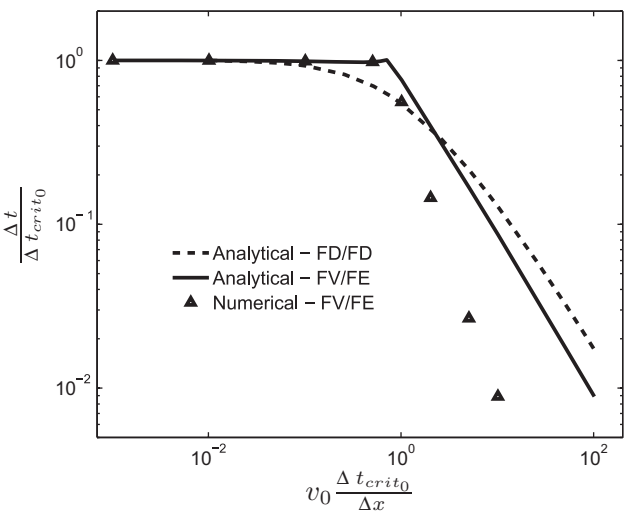

Figure 14. Effect of the interface velocity on the critical time step size for FV/FE discretization. $\Delta x_+ = \Delta x_- = \Delta x$. Δt_{crit_0} denotes the critical value of the time step for a non-moving interface. The FD/FD solution is shown (dashed curve) for comparison.

to the second regime occurs at a smaller values of d_+. Again, the numerical and analytical results match well within the first regime. From this test, it is discovered that the numerical limit on $\eta_\pm$ is approximately 0.65, though the stability criterion suggests no such limit. For $\eta_\pm$ larger, the simulation is unconditionally unstable. This is in contrast with the FD/FD discretization, where the limit on $\eta_\pm$ is 2. The analysis is not able to capture the $\eta_\pm$ limit.

DOI: 10.1002/fld

Figure 14 shows the variation of the time step size with interface velocity. While these parameters are generally not as useful as the non-dimensional r, $d_{\pm}$, and $\eta_{\pm}$, they provide a clearer image of the effect of grid motion on the stability. As in Figure 4, Δt_{crit_0} refers to the critical time step size for the case of a stationary interface. The stability limit of the FD/FD discretization is also included. It clearly shows that for comparatively small interface velocities, the two numerical schemes have essentially the same stability characteristics. However, for larger velocities, the FD method is more stable than the FV/FE discretization.

As in Figure 12(b), the numerical results match the predicted stability limit well within one regime, beyond which the error grows. Below $v_0 \Delta t_{\text{crit}_0}/\Delta x \approx 1$, the error is very small. For larger velocities, the trend of the curve does not fit with the numerical results. However, even within this range, the predicted stability limit can serve as a useful guide in determining a stable time step size.

4. CONCLUSION

A stability study of two explicit coupling schemes has been performed for transient thermal fluid–structure problems. The first scheme involves a FD treatment of both fluid and solid domains, while the second one uses the more common FV/FE combination. The stability analysis has been conducted using the Godunov–Ryabenkii method and the analytical results have been verified numerically. Special emphasis has been placed on the effect of the interface motion on the stability limit, i.e. on the critical size of the time step beyond which the coupled numerical solution becomes unstable.

It has been shown that the interface velocity, v_0, can have a strong effect on the stability of the explicit coupling scheme: the higher the value of v_0, the smaller the critical time step size. The results also indicate that a stable time stepping scheme can be obtained for the FD/FD coupled problem as long as the interface moves by less than two grid spacings per time step. As in the case for stationary interfaces, the most stable coupling scheme involves transferring the heat flux (i.e., a von Neumann boundary condition) from the fluid to the solid and passing the interface temperature (i.e., a Dirichlet boundary condition) from the solid to the fluid.

The stability criterion for the FV/FE case is more complex than that of the FD case and involves various instability modes, but the overall dependence of the critical time step size on the interface velocity is very similar. For small values of v_0, the critical time step size remains independent on the amplitude of the interface velocity. When the ratio between v_0 and the grid spacing becomes comparable to the critical time step size in the absence of interface motion, the critical size of the time step decays rapidly with increasing interface velocity. In that regime, the FV/FE discretization appears to be much less stable than its FD/FD counterpart.

REFERENCES

1. Johnson HB, Seipp TG, Candler GV. Numerical study of hypersonic reacting boundary layer transition on cones. *Physics of Fluids* 1998; **10**(10):2676–2685.
2. Sondak SL, Dorney DJ. Simulation of coupled unsteady flow and heat conduction in turbine stage. *AIAA Journal of Propulsion and Power* 2000; **16**(6):1141–1148.
3. Heselhaus A. A hybrid coupling scheme and stability analysis for coupled solid/fluid turbine blade temperature prediction. *Paper 98-GT-088*, ASME Turbo Expo'98, Stockholm, Sweden, 1998.

DOI: 10.1002/fld

4. Lee I, Roh JH, Oh IK. Aerothermoelastic phenomena of aerospace and composite structures. *Journal of Thermal Stresses* 2003; **26**(6):525–546.
5. Alavilli PJ, Buckmaster J, Jackson T, Short M. Ignition-transient modeling for solid propellant rocket motors. *AIAA 2000-3567*, *36th AIAA/ASME/SAE/ASEE Joint Propulsion Conference and Exhibit*, Huntsville, AL, July 2000.
6. Fiedler RA, Haselbacher A, Breitenfeld MS, Alexander P, Masa L, Ross WC. 3D simulations of ignition transients in the RSRM. *AIAA Paper 2005-3993*, *41st AIAA/ASME/SAE/ASEE Joint Propulsion Meeting and Exhibit*, Tucson, 2005.
7. Giles MB. Stability analysis of numerical interface conditions in fluid–structure thermal analysis. *International Journal for Numerical Methods in Fluids* 1997; **25**:421–436.
8. Jackson TL, Massa L, Brewster MQ. Unsteady combustion modelling of energetic solids, revisited. *Combustion Theory and Modelling* 2004; **8**:513–532.
9. Godunov SK, Ryabenkii VS. *The Theory of Difference Schemes—An Introduction*. North-Holland: Amsterdam, 1964.
10. Sousa E. Stability analysis of difference methods for parabolic initial value problems. *Journal of Scientific Computing* 2004; **26**(1):45–66.

DOI: 10.1002/fld